Soft Matter

Cite this: *Soft Matter*, 2012, **8**, 3463

www.rsc.org/softmatter

PAPER

Lamellar microdomain orientation and phase transition of polystyrene-*b*-poly (methyl methacrylate) films by controlled interfacial interactions†

Seunghoon Choi,[a] Eunhye Kim,[a] Hyungju Ahn,[a] Sudhakar Naidu,[a] Yonghoon Lee,[a] Du Yeol Ryu,*[a] Craig J. Hawker[b] and Thomas P. Russell[c]

Received 3rd December 2011, Accepted 11th January 2012
DOI: 10.1039/c2sm07297a

The orientation of lamellar microdomains and phase transition for the thin films of a symmetric polystyrene-*b*-poly(methyl methacrylate) (PS-*b*-PMMA) on random copolymer-grafted substrates were investigated by transmission electron microscopy (TEM) and grazing-incidence small-angle X-ray scattering (GISAXS). The styrene mole fraction (X_S) in random copolymers of P(S-*r*-MMA) was controlled to tune the interfacial interactions at the substrates from PS-selective to PMMA-selective. Except in the case of a neutral substrate with $X_S = 0.55$, all the films showed the parallel orientations of lamellar microdomains, which were validated by the TEM images. However, the GISAXS analysis of PS-*b*-PMMA films indicated that the intensity ratio of the *out-of-plane* scattering to the *in-plane* scattering can be a sensitive indicator for evaluating the degree of orientation of lamellar microdomains or surface neutrality at the substrates. The orientation of lamellar microdomains on a neutral substrate was influenced by the film thickness and molecular weight of PS-*b*-PMMA, which results from predominantly the entropic contribution to the free energy in competition between the chain-end effect and nematic term. Intriguingly, the order-to-disorder temperature (ODT) of PS-*b*-PMMA films on a series of the substrates shows a minimum at $X_S = 0.55$. The ODT measurements, a new approach to evaluating the interfacial interactions at substrates, confirm that a neutral substrate induces surface compatibility between the PS and PMMA blocks at the substrate.

Introduction

The self-assembly of block copolymer (BCP) embraces a wide range of interesting physics with potential applications in nanoscopic pattern transfer.[1–5] A diblock copolymer, consisting of two polymer chains covalently linked together, can self-assemble into ordered arrays of nanoscopic microdomains, including lamellar, gyroid, cylindrical, and spherical microdomains depending on the volume fraction, the total number of segments (N), the Flory–Huggins segmental interaction parameter (χ) between the two blocks, and the chain rigidity.[1,6–10] With increasing temperature, if the product of χN decreases below a critical value ($\chi N = 10.495$ for symmetric BCP), the BCP undergoes a transition from the ordered to the disordered state, and thus microphase-separates when the temperature decreases.[11]

For the BCP films confined at interfaces, the phase behavior and orientation of microdomains will be influenced by (i) the interfacial interactions at both air/polymer and polymer/substrate interfaces and (ii) the commensurability between the equilibrium period (L_0) of the BCP and the total film thickness.[12–17] The large difference in surface energy of the two blocks and/or a preferential interaction of the substrate towards one block resulted in preferential segregation of one block to either air/polymer or polymer/substrate interfaces, or both, which forces the parallel orientation of microdomains.[18–24] For this reason, the technology for directing orientation of microdomains in the BCP films has been developed by many researchers *via* the chemical modification of substrates, roughened substrates, and the application of external fields.[25–33]

A functional random copolymer approach to tune the interfacial interactions at substrates was successful to achieve the perpendicular orientation of lamellar and cylindrical microdomains on neutral (or non-selective) substrates.[14,34–43] Particularly in the substrates modified with random copolymers of poly (styrene-*r*-methyl methacrylate) (P(S-*r*-MMA)), surface neutrality at the substrates with the PS and PMMA blocks can be correlated with $\Delta\gamma = |\gamma_{As} - \gamma_{Bs}| \approx 0$, where $\Delta\gamma$ is the difference

[a]*Department of Chemical and Biomolecular Engineering, Yonsei University, 50 Yonsei-ro, Seodaemun-gu, Seoul 120-749, Korea. E-mail: dyryu@yonsei.ac.kr; Fax: +822 312 6401; Tel: +822 2123 5756*
[b]*Material Research Laboratory and Departments of Materials, Chemistry and Biochemistry, University of California, Santa Barbara, CA 93016, USA*
[c]*Department of Polymer Science & Engineering, University of Massachusetts, Amherst, MA 01003, USA*

† Electronic supplementary information (ESI) available: The GISAXS pattern for a disordered BCP film. See DOI: 10.1039/c2sm07297a

in interfacial energy of the substrate with the A and B blocks. When the interfacial interactions with the PS and PMMA blocks are balanced in thin film geometry, then the only frustration associated with the incommensurability between the period of the BCP (L_0) and the film thickness resulted in the perpendicular orientation of microdomains.[44,45] The optimal styrene mole fraction (X_S) in P(S-*r*-MMA) that balances the interfacial interactions at substrates was determined experimentally to be ~0.64 and ~0.55 for cylindrical and lamellar morphologies in PS-*b*-PMMA films, respectively.[44] More interestingly, the thickness-dependent transition behavior of the BCP films indicated that the order-to-disorder temperature (ODT) in the thin films was significantly influenced by the interfacial interactions at substrates.[17,46–48]

In the present study, we systematically investigated the orientation of lamellar microdomains and phase transition for the thin films of PS-*b*-PMMA. This study takes advantage of the random copolymer approach to control the interfacial interactions at substrates from PS-selective to PMMA-selective. A parallel orientation of lamellar microdomains was observed in the BCP films all over the composition of P(S-*r*-MMA)-grafted substrates, except in the case of a neutral substrate that induces surface compatibility between the PS and PMMA blocks in the weak segregation regime. We showed that the grazing-incidence small-angle X-ray scattering (GISAXS) analysis can be a sensitive indicator for evaluating the degree of orientation of lamellar microdomains or surface neutrality at the substrates. The orientation of lamellar microdomains on a neutral substrate was influenced by the film thickness and molecular weight of BCP, which results from predominantly the entropic contribution to the free energy in competition between the chain-end effect and nematic term. Intriguingly, the ODT of PS-*b*-PMMA films on a series of the substrates shows a minimum at $X_S = 0.55$. The ODT measurements, a new approach to evaluating the interfacial interactions at substrates, confirm that a neutral substrate induces surface compatibility between the PS and PMMA blocks at the substrate.

Experimental section

A nearly symmetric PS-*b*-PMMA was purchased from Polymer Source with the number-averaged molecular weight (M_n) and polydispersity index (M_w/M_n), characterized by size-exclusion chromatography (SEC), of 29 000 g mol^{-1} and 1.08, respectively. The volume fraction of PS (ϕ_{PS}) in the BCP was determined to be 0.553 by ^{1}H nuclear magnetic resonance (^{1}H-NMR) based on the mass densities of two components (1.05 and 1.184 g cm^{-3} for PS and PMMA, respectively). For comparison, the three symmetric PS-*b*-PMMAs ($\phi_{PS} = 0.500$) with M_n = 50 000, 74 000, and 113 000 g mol^{-1} ($M_w/M_n < 1.06$) were synthesized by sequential anionic polymerization of styrene and methyl methacrylate in tetrahydrofuran (THF); this was performed at −78 °C in the presence of LiCl (high purity, Aldrich), under purified argon, and using *sec*-butyllithium as an initiator. The hydroxyl end-functionalized random copolymers composed of styrene and methyl methacrylate, P(S-*r*-MMA)s, were synthesized by a nitroxide-mediated living free radical polymerization.[25] The M_n and M_w/M_n of P(S-*r*-MMA)s are approximately 10 000 g mol^{-1} and less than 1.50, respectively. The styrene mole fraction (X_S) in the random copolymers was varied so as to control the interfacial interactions at substrates.

Grafting to the substrate was achieved by thermally annealing the thin films of end-functionalized P(S-*r*-MMA)s on standard Si wafers at 170 °C for 3 days under vacuum, well above the glass transition temperatures (T_gs) of PS and PMMA (100 and 115 °C, respectively) for 3 days. During this process, end-functional hydroxyl groups of random copolymers can diffuse to the polymer/substrate interface and react with functional groups (predominantly hydroxyl groups) on the native oxide layer, leading to polymer chains covalently anchored to the substrate.[25] The grafting thickness of P(S-*r*-MMA)s was measured to be ~5 ± 0.3 nm by ellipsometry (SE MG-1000, Nano-view Co.) at an incidence angle of 70° after rinsing in toluene to remove the unanchored polymer chains on the substrate. The ODT and equilibrium period (L_0) of PS-*b*-PMMA (M_n = 29 000 g mol^{-1}) are 200 °C and 19.6 nm, respectively, as measured by small-angle X-ray scattering (SAXS). The BCP films were also annealed at 170 °C for 3 days under vacuum to obtain thermal equilibrium.

Grazing-incidence small-angle X-ray scattering (GISAXS) experiments were carried out at the 4C2 beam-line of the Pohang Accelerator Laboratory (PAL), Pohang, Korea. The operating conditions were set at a wavelength of 1.38 Å and a sample-to-detector distance of 2.2 m. The film samples were mounted in a heating cell under vacuum and the incident angle (α_i) was set at 0.160°, well above the critical angle (0.156°) of PS-*b*-PMMA films. All the heating experiments were automatically controlled with a PID temperature controller from 160 to 250 °C at a constant heating rate of 1 °C min^{-1}. To minimize sample degradation by the X-ray beam, a minimal exposure time of 10–20 s was used.

The cross-sectional structures of PS-*b*-PMMA films were investigated by transmission electron microscopy (TEM; S-7600, Hitachi) with an accelerating voltage of 80 kV. A thin carbon layer was first evaporated at the air/polymer interface, followed by being embedded with epoxy resin (Araldite 502, Polysciences). The polymer/substrate interface was again treated with a thin carbon layer and epoxy resin in a similar manner. Thin sections (~50 nm) from the epoxy-embedded film were obtained using an Ultra Microtome (RMC PTXL) with a diamond knife at room temperature. To enhance the electron density contrast between two phases, the PS block was selectively stained with RuO_4.

Results and discussion

The surface modification was well controlled by grafting hydroxyl-terminated P(S-*r*-MMA)s to the substrate. The styrene mole fraction (X_S) in P(S-*r*-MMA) ranges from 0.20 to 0.85; this tunes the interfacial interactions at substrates from PS-selective to PMMA-selective. The BCP films were spin-coated from toluene solution onto P(S-*r*-MMA)-grafted substrates and thermally annealed at 170 °C for 3 days under vacuum before measurements. A previous study demonstrated that the ODT of PS-*b*-PMMA films on particularly a neutral substrate reveals thickness dependence when the thickness is less than $20L_0$.[48] For this reason, the effective film thicknesses in this study were set at $12L_0$ (235 nm) and $15L_0$ (294 nm) within the limit of the influence of the interfacial interactions at substrates.

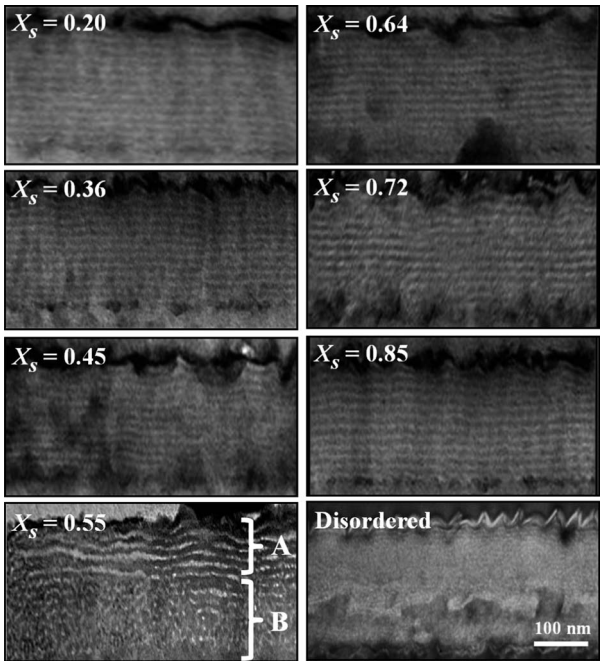

Fig. 1 The cross-sectional TEM images for PS-*b*-PMMA films ($12L_0$) on P(S-*r*-MMA)-grafted substrates, where the styrene mole fraction (X_S) in P(S-*r*-MMA) ranges from 0.20 to 0.85. For comparison, the last image indicates a disordered BCP film. The scale bar in TEM images indicates 100 nm.

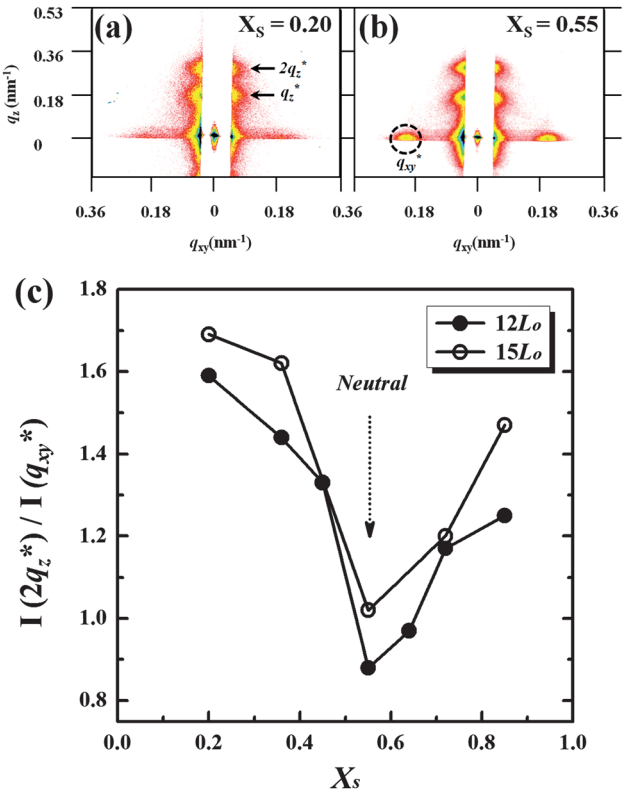

Fig. 2 The 2D GISAXS patterns for PS-*b*-PMMA films ($12L_0$) on P(S-*r*-MMA)-grafted substrates with (a) $X_S = 0.20$ and (b) $X_S = 0.55$. (c) The intensity ratio of the *out-of-plane* scattering (at $2q_z^*$) to the *in-plane* scattering (at q_{xy}^*) from the GISAXS patterns; this is shown as a function of X_S at the substrates for the BCP films with thicknesses of $12L_0$ and $15L_0$.

Fig. 1 shows the cross-sectional transmission electron microscopy (TEM) images for PS-*b*-PMMA films ($12L_0$) on P(S-*r*-MMA)-grafted substrates. For the thin films on the substrates with $X_S = 0.20$ to 0.45, the TEM images display the lamellar microdomains oriented parallel to the substrate throughout the films. The PS block with lower surface energy tends to migrate into the air/polymer interface and the PMMA block prefers to interact with PMMA-selective (or preferential) substrates; this preferentially forces the lamellar microdomains to be oriented parallel to the substrate. However, for the substrate with $X_S = 0.55$, the parallel orientation of lamellar microdomains was preserved in the top half (marked A), while a loss of lamellar microdomains was seen in the bottom half (marked B). Particularly in the case of a neutral substrate, it can be attributed to surface compatibility between the PS and PMMA blocks at the substrate, leading to a short-range ordered structure of the BCP in the weak segregation regime ($\chi N = 11.97$ on the basis of ref. 49). The image is also distinguished from the featureless TEM image of a disordered BCP film (in the last image). As X_S further increases to 0.85 (approaching to PS-selective), the lamellar microdomains were again oriented parallel to the substrate, since both air/polymer and polymer/substrate interfaces were selectively favorable to the PS block.

Note that the TEM characterization is limited to the local area of nanoscopic level morphology, even though it provides credible information. For more statistically averaged information, 2D GISAXS was used in this study. Fig. 2a and b show the GISAXS patterns for PS-*b*-PMMA films on the substrates with $X_S = 0.20$ and 0.55, respectively. In the grazing-incidence scattering geometry, q_{xy} is the *in-plane* scattering vector parallel to the sample surface (or normal to the incidence plane), where the *d*-spacing of the BCP film is directly related to the maximum peak position of q_{xy}^* by $d = 2\pi/q_{xy}^*$. q_z is the *out-of-plane* scattering vector normal to the sample surface based on the reflected beam, defined by $q_z = (4\pi/\lambda)\sin\theta$. Incident angle ($\alpha_i$) in GISAXS was set at 0.160° above the critical angle (0.156°) for PS-*b*-PMMA films to probe morphology across the entire film thickness.

In the GISAXS pattern of the thin film on the substrate with $X_S = 0.20$, two characteristic *out-of-plane* reflections (indicated by q_z^* and $2q_z^*$) along q_z near the vertical beam-stop at $q_{xy} = 0$ can be correlated to the parallel orientation of lamellar microdomains. These q_z^* and $2q_z^*$ peaks were preserved in the thin films on the substrate with $X_S = 0.55$. However, the q_{xy}^* peak was also intensified, which presumably arises from a short-range ordered structure of the BCP films, not from a disordered state. For comparison, a disordered BCP film at elevated temperature (~200 °C) exhibits two arc-shaped diffuse scattering patterns arising from a correlation hole scattering by compositional fluctuations (ESI†).

The intensity ratio of the *out-of-plane* scattering (at $2q_z^*$) to the *in-plane* scattering (at q_{xy}^*) from the GISAXS patterns was characterized as a function of X_S at the substrates, as shown in Fig. 2c. Indeed, it suggests a quantitative analysis to evaluate the degree of orientation of lamellar microdomains, because the $2q_z^*$ peak (consistently with q_z^* peak) reflects the parallel

orientation of lamellar microdomains and the q_{xy}* peak arises from a short-range ordered structure of the BCP films (or a loss of lamellar microdomains). At first, the intensity ratio decreases with increasing X_S and then increases, leading to a minimum at $X_S = 0.55$ that corresponds to the specific thin film having a condition of surface compatibility between the PS and PMMA blocks at the substrate. Moreover, at slightly asymmetric X_S, it indicates the high sensitivity to the variation of the interfacial interactions at the substrates. In comparison to the TEM images, where all the films showed the parallel orientations of lamellar microdomains except in the case of a neutral substrate, this analysis is worthy of note in that the intensity ratio can be a sensitive indicator for evaluating the degree of orientation of lamellar microdomains or surface neutrality at the substrates.

Fig. 3 shows the TEM images for PS-*b*-PMMA films ($15L_0$ and $40L_0$ (780 nm)) on a neutral substrate with $X_S = 0.55$. Interestingly, a slight increase in the film thickness to $15L_0$ led to an increase (~70%) in the parallel orientation of lamellar microdomains (marked A) and a decrease in a short-range ordered structure of the BCP films. Increasing the film thickness to $40L_0$ resulted in a parallel orientation of lamellar microdomains over the film, which is consistent with the prior result.[48] In addition, the molecular weight of PS-*b*-PMMA was increased, in which the product of χN can be a measure of the segregation between the two blocks. A recently reported χ for PS-*b*-PMMA was used in calculation[49] by

$$\chi = -0.0033 + 20.0718/T \quad (1)$$

Three additional symmetric PS-*b*-PMMAs with $M_n = 50\,000$, 74 000, and 113 000 g mol^{-1} were subjected to the thin films with the consistent thickness of ~$12L_0$ on a neutral substrate, and thermally annealed at 170 °C, 180 °C, and 210 °C, respectively, which are the lowest temperatures for an equilibrium. The molecular weight dependence of the orientation of lamellar microdomains is shown in Fig. 4 by the TEM images. For the thin film with $M_n = 50\,000$ g mol^{-1} ($\chi N = 20.60$), a neutral substrate led to dominantly the parallel orientation of lamellar microdomains and the perpendicular orientation near the polymer/substrate interface. There was no short-range ordered structure that arises from surface compatibility between the PS and PMMA blocks at the substrate. As the molecular weight increases (from $\chi N = 29.73$ to 42.40; Fig. 4b and c), the population of the perpendicular orientation near the polymer/substrate interface significantly increases, which is caused by a neutral substrate that balances the interfacial interactions with the PS and PMMA blocks.

To describe the orientation of lamellar microdomains, we used a theoretical approach suggested by Pickett *et al.*[12,50,51] The difference in the free energy between the parallel and perpendicular orientations, $\Delta = E_{\parallel} - E_{\perp}$, can be expressed by

$$\Delta = \Delta_w + \Delta_n + \Delta_e \propto -c_w + c_n N^{-2/3} - c_e N^{-8/9} \quad (2)$$

where Δ_w, Δ_n, and Δ_e are the enthalpic interaction, nematic, and chain-end effect terms, respectively, and c_is are coefficients for each term. The last two terms are the entropic contribution

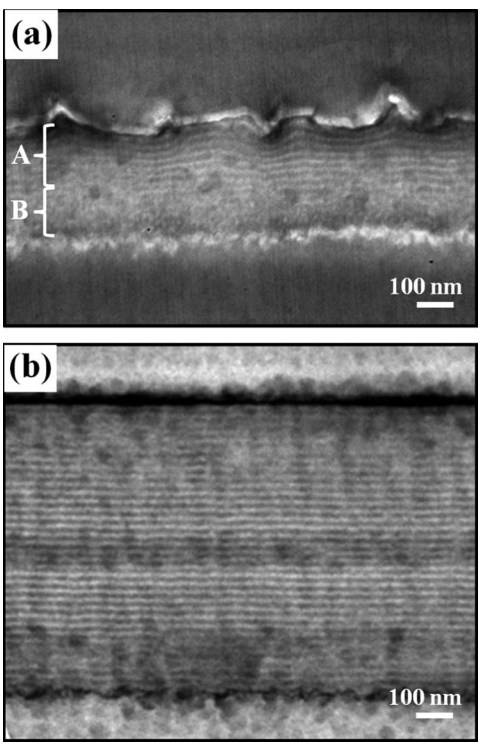

Fig. 3 The cross-sectional TEM images for PS-*b*-PMMA ($M_n = 29\,000$ g mol^{-1}) films with thicknesses of (a) $15L_0$ and (b) $40L_0$ on a neutral substrate with $X_S = 0.55$.

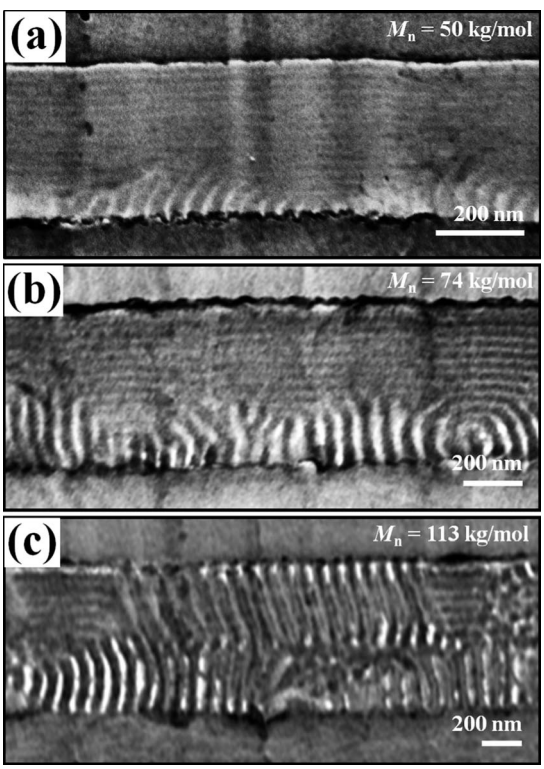

Fig. 4 The cross-sectional TEM images for PS-*b*-PMMA films (~$12L_0$) on a neutral substrate with $X_S = 0.55$, where the molecular weights of PS-*b*-PMMA are (a) 50 000, (b) 74 000, and (c) 113 000 g mol^{-1}.

associated with the molecular weight of BCP. Especially in the thin films on a neutral substrate, the first enthalpic interaction term is minor because the difference in surface energy of the two blocks is small (40.7 and 41.1 mN m^{-1} for PS and PMMA, respectively).[52] At low N, the chain-end effect dominates the nematic term of stretched chains at the substrate, resulting in a negative value of Δ favoring the parallel orientation of lamellar microdomains. It may suppress the balanced interfacial interactions even at a neutral substrate, as similarly demonstrated in Fig. 3 by the thickness dependence of PS-*b*-PMMA films in the weak segregation regime ($\chi N = 11.97$).

With increasing N, however, the nematic term of stretched chains at the substrate dominates the chain-end effect, where a positive value of Δ favors the perpendicular orientation of lamellar microdomains. Accordingly, the molecular weight dependence of PS-*b*-PMMA films on a neutral substrate shows that the chain stretching of the BCP with increasing N is entropically favorable to the perpendicular orientation of lamellar microdomains. In fact, the parallel orientation of lamellar microdomains tends to originate from the air/polymer interface, as shown in Fig. 4 by the TEM images, indicating that the difference in surface energy of the two blocks may still be effective though minor.

To determine the ODT of the BCP films, *in situ* 2D GISAXS patterns were measured for PS-*b*-PMMA films on a series of the substrates, at which the patterns were taken at each temperature during heating from 160 to 240 °C at a rate of 1 °C min^{-1}. Two characteristic changes occur at transition:[48] the *out-of-plane* reflections (along q_z) correlated to the parallel orientation of lamellar microdomains weaken with increasing temperature ($T >$ ODT) and the *in-plane* scattering peaks (along q_{xy}) intensify with two broad maxima on two arc-shaped diffuse scattering patterns due to a disordered state (ESI†). Fig. 5 shows the intensity profiles in the *in-plane* scattering peaks (at q_{xy}*) from the GISAXS patterns for the BCP ($12L_0$) films on the substrates, which were scanned along q_{xy} at constant $q_z = 0$. The temperature dependence of the *in-plane* scattering peaks allows us to determine the ODTs by the discontinuous changes due to the structural transition into a disordered film. It should be noted that this analysis is reasonably consistent with the direct analysis for peak (q_{xy}*) position and full-width at half-maximum (FWHM) of the GISAXS patterns. A remarkable decrease in ODT was observed for PS-*b*-PMMA film on a neutral substrate with $X_S = 0.55$, whereas at more asymmetric compositions of P(S-*r*-MMA)-grafted substrates, the ODT increased.

Fig. 6 summarizes the ODT of PS-*b*-PMMA films as a function of X_S at the substrates. Because the film thicknesses were set at $12L_0$ and $15L_0$, phase transition reflects the influence of the interfacial interactions at substrates. For the more sensitive thin films with a thickness of $12L_0$, the higher ODT of ~218 °C was seen at the substrates with $X_S = 0.20$ and 0.36. It can be attributed to the suppression of compositional fluctuations normal to the substrate, because the dominant orientation of the lamellar microdomains was found to be parallel to the substrate. The ODT then decreases at the substrate with $X_S = 0.45$, even though the parallel orientation of the lamellar microdomains is preserved (shown in Fig. 1). A minimum (~200 °C) of the ODT was observed at the substrate with $X_S = 0.55$, indicating surface compatibility between the PS and PMMA blocks at the substrate. It may be correlated to a consequence of a short-range ordered structure of the BCP film in the weak segregation regime.

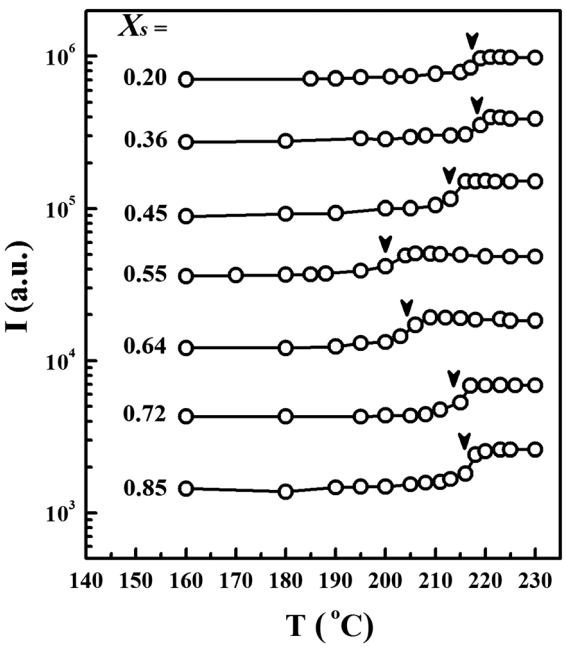

Fig. 5 The intensity profiles in the *in-plane* scattering peaks (at q_{xy}*) from the GISAXS patterns for PS-*b*-PMMA films ($12L_0$) depending on X_S at the substrates. The profiles were scanned along q_{xy} at constant $q_z = 0$. The points indicate the ODTs for PS-*b*-PMMA films by the discontinuous changes due to the structural transition into a disordered film.

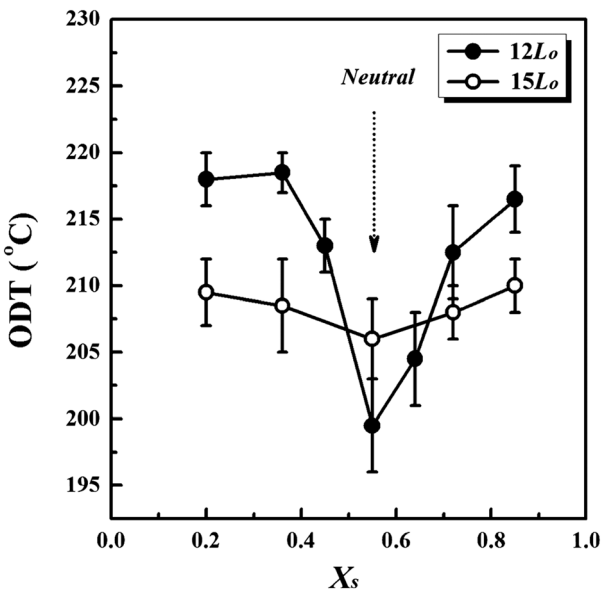

Fig. 6 The ODT of PS-*b*-PMMA films with thicknesses of $12L_0$ and $15L_0$ as a function of X_S at the substrates. These transition temperatures were determined at the midpoints of the discontinuous range in intensities. Error bars indicate the initial and final points of transition temperatures.

On further increasing X_S to 0.85, the ODT increases again, because the PS-selective substrates in turn promote the parallel orientation of the lamellar microdomains, as is the opposite case at the substrates with $X_S = 0.20$ and 0.36. When the film thickness increases to $15L_0$, a minimum of the ODT was observed at the same substrate with $X_S = 0.55$, although the influence of the interfacial interactions at substrates was diminished. This quantitative analysis allows us to measure the interfacial interactions at substrates more accurately, and confirm a neutral substrate that induces surface compatibility between the PS and PMMA blocks at the substrate. The ODT result is in parallel with the analysis for the intensity ratio of the *out-of-plane* scattering to the *in-plane* scattering from the GISAXS patterns measured at room temperature.

Conclusions

In this study, we investigated the orientation of lamellar microdomains and phase transition for the thin films of PS-*b*-PMMA (M_n = 29 000 g mol^{-1}; $\chi N = 11.97$) on P(S-*r*-MMA)-grafted substrates, where the film thicknesses ($12L_0$ and $15L_0$) were within the limit of the influence of the interfacial interactions at substrates. The styrene mole fraction (X_S) in P(S-*r*-MMA) was controlled to tune the interfacial interactions at the substrates from PS-selective to PMMA-selective. In the TEM characterization, a loss of lamellar microdomains (a short-range ordered structure) on a neutral substrate was observed in the thin films with thicknesses of $12L_0$ and $15L_0$, which can be attributed to surface compatibility between the PS and PMMA blocks at the substrate. Except in the case of a neutral substrate, all the films showed the parallel orientations of lamellar microdomains even at asymmetric X_S. However, the GISAXS analysis of PS-*b*-PMMA films indicated that the intensity ratio of the *out-of-plane* scattering to the *in-plane* scattering indicates the high sensitivity to the variation of the interfacial interactions at the substrates; this can be a sensitive indicator for evaluating the degree of orientation of lamellar microdomains or surface neutrality at the substrates.

For PS-*b*-PMMA (M_n = 29 000 g mol^{-1}) films on a neutral substrate, increasing the film thickness to $40L_0$ resulted in a parallel orientation of lamellar microdomains over the film. In addition, when the molecular weight of PS-*b*-PMMA was increased to 113 000 g mol^{-1} ($\chi N = 42.40$) in the thin films, a neutral substrate led to a significant increase in the population of the perpendicular orientation near the polymer/substrate interface. On the basis of a theoretical approach using the difference in the free energy between the parallel and perpendicular orientations, we demonstrated that the orientation of lamellar microdomains on a neutral substrate can be determined predominantly by the entropic contribution to the free energy. In other words, the chain stretching (nematic effect) of the BCP with increasing N is entropically favorable to the perpendicular orientation of lamellar microdomains, whereas at low N, it was dominated by the chain-end effect favoring the parallel orientation of lamellar microdomains.

Intriguingly, for PS-*b*-PMMA in the weak segregation regime ($\chi N = 11.97$), the ODT of the thin films on a series of P(S-*r*-MMA)-grafted substrates shows a minimum at $X_S = 0.55$, as a consequence of surface compatibility between the PS and PMMA blocks at the substrate. Therefore, the result indicates that the ODT measurements, a new approach to evaluating the interfacial interactions at substrates, confirm that a neutral substrate with $X_S = 0.55$ induces surface compatibility between the PS and PMMA blocks at the substrate, which is also in parallel with the analysis for the intensity ratio of the *out-of-plane* scattering to the *in-plane* scattering from the GISAXS patterns measured at room temperature.

Acknowledgements

This work was supported by the Nuclear R&D Programs, NRF grant (2011-0022690), and APCPI ERC program (R11-2007-050-00000) funded by the Ministry of Education, Science & Technology (MEST), Korea, as well as by the NSF MRSEC program (MRL at UCSB) under Award no. DMR-112105.

References

1 I. W. Hamley, *The Physics of Block Copolymers*, Oxford University Press, New York, 1998.
2 C. Park, J. Yoon and E. L. Thomas, *Polymer*, 2003, **44**, 6725–6760.
3 J. Bang, U. Jeong, D. Y. Ryu, T. P. Russell and C. J. Hawker, *Adv. Mater.*, 2009, **21**, 4769–4792.
4 I. W. Hamley, *Prog. Polym. Sci.*, 2009, **34**, 1161–1210.
5 E. B. Gowd, B. Nandan, N. C. Bigall, A. Eychmüller, P. Formanek and M. Stamm, *Polymer*, 2010, **51**, 2661–2667.
6 I. W. Hamley, K. A. Koppi, J. H. Rosedale, F. S. Bates, K. Almdal and K. Mortensen, *Macromolecules*, 1993, **26**, 5959–5970.
7 S. Foerster, A. K. Khandpur, J. Zhao, F. S. Bates, I. W. Hamley, A. J. Ryan and W. Bras, *Macromolecules*, 1994, **27**, 6922–6935.
8 A. K. Khandpur, S. Foerster, F. S. Bates, I. W. Hamley, A. J. Ryan, W. Bras, K. Almdal and K. Mortensen, *Macromolecules*, 1995, **28**, 8796–8806.
9 M. W. Matsen and F. S. Bates, *Macromolecules*, 1996, **29**, 1091–1098.
10 M. W. Matsen and F. S. Bates, *J. Chem. Phys.*, 1997, **106**, 2436–2448.
11 L. Leibler, *Macromolecules*, 1980, **13**, 1602–1617.
12 G. T. Pickett, T. A. Witten and S. R. Nagel, *Macromolecules*, 1993, **26**, 3194–3199.
13 P. Mansky and T. P. Russell, *Macromolecules*, 1995, **28**, 8092–8095.
14 E. Huang, S. Pruzinsky, T. P. Russell, J. Mays and C. J. Hawker, *Macromolecules*, 1999, **32**, 5299–5303.
15 J.-U. Sommer, A. Hoffmann and A. Blumen, *J. Chem. Phys.*, 1999, **111**, 3728–3732.
16 I. I. Potemkin, *Macromolecules*, 2004, **37**, 3505–3509.
17 A. B. Croll, A.-C. Shi and K. Dalnoki-Veress, *Phys. Rev. E: Stat., Nonlinear, Soft Matter Phys.*, 2009, **80**, 051803.
18 H. Hasegawa and T. Hashimoto, *Macromolecules*, 1985, **18**, 589–590.
19 C. S. Henkee, E. L. Thomas and L. J. Fetters, *J. Mater. Sci.*, 1988, **23**, 1685–1694.
20 S. H. Anastasiadis, T. P. Russell, S. K. Satija and C. F. Majkrzak, *Phys. Rev. Lett.*, 1989, **62**, 1852.
21 G. Coulon, T. P. Russell, V. R. Deline and P. F. Green, *Macromolecules*, 1989, **22**, 2581–2589.
22 T. P. Russell, G. Coulon, V. R. Deline and D. C. Miller, *Macromolecules*, 1989, **22**, 4600–4606.
23 E. Buck and J. Fuhrmann, *Macromolecules*, 2001, **34**, 2172–2178.
24 T. Xu, C. J. Hawker and T. P. Russell, *Macromolecules*, 2005, **38**, 2802–2805.
25 P. Mansky, Y. Liu, E. Huang, T. P. Russell and C. J. Hawker, *Science*, 1997, **275**, 1458–1460.
26 G. Kim and M. Libera, *Macromolecules*, 1998, **31**, 2569–2577.
27 L. Rockford, Y. Liu, P. Mansky, T. P. Russell, M. Yoon and S. G. J. Mochrie, *Phys. Rev. Lett.*, 1999, **82**, 2602–2605.
28 T. Thurn-Albrecht, R. Steiner, J. DeRouchey, C. M. Stafford, E. Huang, M. Bal, M. Tuominen, C. J. Hawker and T. P. Russell, *Adv. Mater.*, 2000, **12**, 787–791.
29 B. H. Sohn and S. H. Yun, *Polymer*, 2002, **43**, 2507–2512.
30 E. Sivaniah, Y. Hayashi, M. Iino, T. Hashimoto and K. Fukunaga, *Macromolecules*, 2003, **36**, 5894–5896.

31 V. Olszowka, M. Hund, V. Kuntermann, S. Scherdel, L. Tsarkova, A. Boker and G. Krausch, *Soft Matter*, 2006, **2**, 1089–1094.
32 E. J. W. Crossland, S. Ludwigs, M. A. Hillmyer and U. Steiner, *Soft Matter*, 2007, **3**, 94–98.
33 S. Park, D. H. Lee, J. Xu, B. Kim, S. W. Hong, U. Jeong, T. Xu and T. P. Russell, *Science*, 2009, **323**, 1030–1033.
34 P. Mansky, T. P. Russell, C. J. Hawker, M. Pitsikalis and J. Mays, *Macromolecules*, 1997, **30**, 6810–6813.
35 D. Y. Ryu, K. Shin, E. Drockenmuller, C. J. Hawker and T. P. Russell, *Science*, 2005, **308**, 236–239.
36 I. In, Y.-H. La, S.-M. Park, P. F. Nealey and P. Gopalan, *Langmuir*, 2006, **22**, 7855–7860.
37 D. Y. Ryu, J.-Y. Wang, K. A. Lavery, E. Drockenmuller, S. K. Satija, C. J. Hawker and T. P. Russell, *Macromolecules*, 2007, **40**, 4296–4300.
38 J. Bang, J. Bae, P. Löwenhielm, C. Spiessberger, S. Given-Beck, T. Russell and C. Hawker, *Adv. Mater.*, 2007, **19**, 4552–4557.
39 E. Han, K. O. Stuen, Y.-H. La, P. F. Nealey and P. Gopalan, *Macromolecules*, 2008, **41**, 9090–9097.
40 E. Han and P. Gopalan, *Langmuir*, 2009, **26**, 1311–1315.
41 S. Ji, C.-C. Liu, W. Liao, A. L. Fenske, G. S. W. Craig and P. F. Nealey, *Macromolecules*, 2011, **44**, 4291–4300.
42 T. Vu, N. Mahadevapuram, G. M. Perera and G. E. Stein, *Macromolecules*, 2011, **44**, 6121–6127.
43 C. Boyer, M. H. Stenzel and T. P. Davis, *J. Polym. Sci., Part A: Polym. Chem.*, 2011, **49**, 551–595.
44 S. Ham, C. Shin, E. Kim, D. Y. Ryu, U. Jeong, T. P. Russell and C. J. Hawker, *Macromolecules*, 2008, **41**, 6431–6437.
45 D. Y. Ryu, S. Ham, E. Kim, U. Jeong, C. J. Hawker and T. P. Russell, *Macromolecules*, 2009, **42**, 4902–4906.
46 C. Shin, H. Ahn, E. Kim, D. Y. Ryu, J. Huh, K.-W. Kim and T. P. Russell, *Macromolecules*, 2008, **41**, 9140–9145.
47 E. Kim, H. Ahn, D. Y. Ryu, J. Kim and J. Cho, *Macromolecules*, 2009, **42**, 8385–8391.
48 E. Kim, S. Choi, R. Guo, D. Y. Ryu, C. J. Hawker and T. P. Russell, *Polymer*, 2010, **51**, 6313–6318.
49 H. Ahn, D. Y. Ryu, Y. Kim, K. W. Kwon, J. Lee and J. Cho, *Macromolecules*, 2009, **42**, 7897–7902.
50 P. Busch, D. Posselt, D.-M. Smilgies, B. Rheinländer and F. Kremer, *Macromolecules*, 2003, **36**, 8717–8727.
51 P. Busch, D. Posselt, D. M. Smilgies, M. Rauscher and C. M. Papadakis, *Macromolecules*, 2007, **40**, 630–640.
52 D. Chen, Y. Gong, H. Huang, T. He and F. Zhang, *Macromolecules*, 2007, **40**, 6631–6637.